Leveraging Multiple Connected Traffic Light Signals in an Energy-Efficient Speed Planner

Jihun Han, Daliang Shen, Dominik Karbowski, and Aymeric Rousseau, *Member, IEEE*

***Abstract*—Connecting automated vehicles to traffic lights can lead to significant energy savings by enabling them to pass through intersections in an energy-efficient way without unnecessary stops. A cellular-based communication system connecting multiple traffic lights can help realize the full potential of energy-efficient driving at intersections. Thus, we propose a hierarchical speed planner that can leverage information from multiple connected traffic lights. The proposed speed planner consists of two modules: a green window selector and a reference trajectory generator. The green window selector, based on Dijkstra's algorithm, finds a series of "green windows" for connected traffic lights that builds an energy-optimal path for vehicles to follow. The reference trajectory generator finds optimal entering times, based on the selected green window at each intersection, and then computes reference trajectories. Deriving and using analytical optimal entering speeds as a function of entering times allows us to guarantee the computational simplicity suitable for real-time implementation. We also demonstrate how to balance energy and traffic flow perspectives in the reference trajectory generator. Finally, a high-fidelity simulation framework is used to evaluate the proposed speed planner and quantify the extent to which it can save energy in various real-world urban route scenarios.**

***Index Terms*—Automotive control, autonomous vehicles, optimal control, optimization algorithms.**

I. Introduction

THE ORIGINAL purpose of vehicle automation technology was to increase vehicle safety and reduce traffic crashes that result in serious injury or death. Automated driver assistance systems (e.g., adaptive cruise control, lane-keeping control) are already available in mass-production vehicles from many original equipment manufacturers (OEMs) [1]. With the development of connectivity technology, energy-efficient driving has attracted considerable attention over recent years. Its potential to save energy without sacrificing safety has been validated in simulations and experiments for various situations (e.g., urban driving with fixed/actuated/non-signalized intersections, highway car-following) [2]. In this letter, we consider urban driving scenarios at fixed signalized intersections with complex traffic rules and focus on the energy-saving potential of energy-efficient driving enabled by connectivity through vehicle-to-infrastructure (V2I) communication.

Broadcasting signal phase and timing (SPaT) information to connected vehicles by V2I may be done by either dedicated short range communication (DSRC) or cellular networks. DSRC-based V2I (DSRC-V2I) guarantees a high maturity/readiness level; however, it can provide limited SPaT information (e.g., the current traffic light state and how long this state will persist). On the other hand, recently introduced cellular-based V2I (C-V2I) is gaining momentum due to its potential to enhance performance (e.g., low latency), reliability (e.g., no packet loss), and coverage (e.g., long range).

Avoiding unnecessary stops at red lights using SPaT information through DSRC-V2I can easily reduce a vehicle's energy consumption when approaching one upcoming traffic light. To optimize its speed trajectory to achieve minimum energy consumption for an entire given trip, a speed planning problem can be formulated and solved by different optimization methods [3]. Powertrain dynamics can be also included in the problem [4]. Different control concepts, such as receding horizon control, have been proposed to enable both eco-approach and eco-departure in the vicinity of a traffic light and have shown significant energy-saving potential [5]–[8]. At the same time, considering multiple traffic lights over the C-V2I range is not trivial, because all red lights must be included as constraints in the speed planning problem. Numerical methods like dynamic programming have been used to tackle these problems in both deterministic (deterministic SPaT) and stochastic (probabilistic SPaT) ways [9]–[13]. The vehicle queue in front of the host vehicle has also been considered in [14].

The existing literature shows that speed adjustment based on the richer SPaT information from a longer connectivity range may facilitate more energy-efficient driving. However, the question of balancing solution optimality and computation efficiency for real-time capability remains. To this end, we proposed a computationally efficient and easy-to-implement-but energy-efficient and robust-speed planner consisting of a *green window selector* and a *reference trajectory generator* as shown in Figure 1. We improve the green window selector by representing each green window by multiple point and thus having a relaxed/larger search space of candidate paths; the energy impact of grade changes between

Manuscript received September 14, 2020; revised November 22, 2020; accepted December 13, 2020. Date of publication December 28, 2020; date of current version March 31, 2021. This work was supported by the U.S. Department of Energy Vehicle Technologies Office under the Systems and Modeling for Accelerated Research in Transportation Mobility Laboratory Consortium, an initiative of the Energy Efficient Mobility Systems Program. Recommended by Senior Editor R. S. Smith. *(Corresponding author: Jihun Han.)*

The authors are with the Energy Systems Division, Argonne National Laboratory, Lemont, IL 60439 USA (e-mail: jihun.han@anl.gov; dshen@anl.gov; dkarbowski@anl.gov; arousseau@anl.gov).

Digital Object Identifier 10.1109/LCSYS.2020.3047605

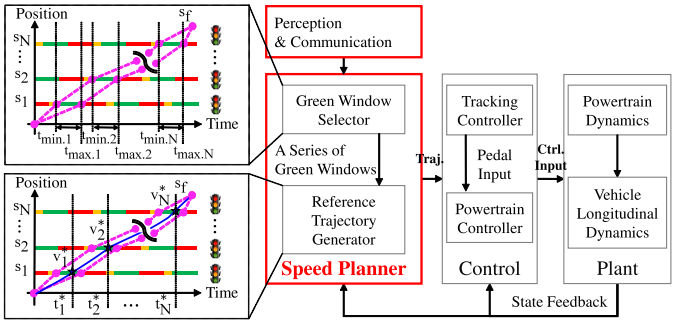

Fig. 1. A schematic diagram of the hierarchical speed planner.

intersections is also taken into account. As for the reference trajectory generator, we derive an analytical solution to a trajectory optimization problem, and use this solution to formulate and solve a parametric optimization problem to find optimal entering-times for the given series of green windows, which significantly reduces computing time. High computational efficiency enables the speed planner to properly react to uncertain situations by updating the reference trajectories fast, and to increase the robustness in real-world driving. Lastly, we evaluate the proposed speed planner for real-world route scenarios and provide insights into the extent to which it saves energy.

This letter is organized as follows: Section II briefly introduce the structure of the proposed speed planner. Sections III and IV present the two essential modules. In Section V, we show simulation study results, and in Section VI, we present our conclusions and future work.

II. Hierarchical Structure

As shown in Figure 1, we proposed the hierarchical structure that can take account of SPaT information from multiple connected intersections. This sequential approach is suitable for online employment in practice although it may not guarantee the global optimality achieved by a concurrent approach. The green window selector on the upper level finds a series of green windows for each intersection. Then, the reference trajectory generator on the lower level computes the reference trajectories, subject to the constraints imposed by the selected green windows. These reference trajectories are fed into a PID tracking controller, which converts this command to pedal position. The pedal position is then the input to the baseline powertrain controller. Finally, vehicle controllers follow the reference trajectories so that the connected and automated vehicles (CAVs) can avoid stops at intersections while driving energy-efficiently.

III. Green Window Selector

A. Model

We consider the following vehicle longitudinal dynamics:

$$\begin{aligned} \dot{s} &= v \\ \dot{v} &= (F_{\text{req}} - c_0 - c_1 v - c_2 v^2 - mg\sin\theta)/m \end{aligned} \tag{1}$$

where s and v are vehicle position and speed, respectively, and F_{req} is the required force at the wheel. Resistive forces include aerodynamic drag, wheel rolling, and hill climbing resistances; coefficients (cs) are determined by vehicle parameters (e.g., aerodynamic drag and rolling resistance coefficients). Parameter m is the vehicle mass, g is the gravity acceleration, and θ is the road slope as a function of the position.

The planned route is divided into a series of road segments by N intersections. We define a set of the following tuples using the position (s_i) and the green light timing, i.e., desired entering time, (t_i) at the i-th intersection:

$$(t_i, s_i) \text{ for } i = 1, \ldots, N. \tag{2}$$

B. Optimization Problem

Let us define the i-th road segment length as $l_i = s_i - s_{i-1}$, where s_0 is origin position. Assuming the piecewise-constant slope and speed limit, the i-th road segment is further divided into n_i sub-segments. The j-th sub-segment of the i-th road segment is characterized with its length ($l_{i,j}$), maximum and minimum speed limits ($v_{\max,i,j}$ and $v_{\min,i,j}$), and slope ($\theta_{i,j}$), for $j = 1, \ldots, n_i$ (See the details in [13]). To reduce the problem's complexity, we assume a piecewise-constant speed trajectory on the planned route. The constant speed $v_{i,j}$ in the j-th sub-segment of the i-th road segment is directly related to the travel time ($t_i - t_{i-1}$), subject to the following condition:[1]

$$\sum_{j=1}^{n_i} \frac{l_{i,j}}{v_{i,j}} = t_i - t_{i-1}, \quad v_{\min,i,j} \le v_{i,j} \le v_{\max,i,j}. \tag{3}$$

Using Equation (1), we first define the static energy consumption over the i-th road segment ($E_{\text{sta},i}$) as follows:

$$E_{\text{sta},i} = \sum_{j=1}^{n_i} l_{i,j}\Big(c_0 + c_1 v_{i,j} + c_2 v_{i,j}^2 + mg\sin\theta_{i,j}\Big) \tag{4}$$

Then, we define dynamic energy consumption ($E_{\text{dyn},i}$), caused by the difference between the constant speeds, as

$$E_{\text{dyn},i} = \sum_{j=1}^{n_i} \frac{1}{2} m\Big(v_{i,j}^2 - v_{i,j-1}^2\Big) k_{\text{recu},i,j} \tag{5}$$

where $v_{i,0} = v_{i-1,n_{i-1}}$, and

$$k_{\text{recu},i,j} = \begin{cases} 1 & \text{if } (v_{i,j}^2 - v_{i,j-1}^2) \ge 0 \\ k_{\text{recu}} & \text{otherwise} \end{cases} \tag{6}$$

Note that the recuperation factor $k_{\text{recu}} \in (0, 1)$ is a constant. Finally, we keep the average speed close to the desired speed v_{des} as follows:

$$J_{\text{t}} = (t_{N+1} - s_{N+1}/v_{\text{des}})^2 \tag{7}$$

where t_{N+1} and s_{N+1} are final travel time and distance to the destination with $t_0 = s_0 = 0$, respectively, and v_{des} is set to a constant value, to define the desired travel time.

In summary, the following optimization problem is formulated to find the series of t_i subject to the feasible set $\mathfrak{T}_i$ for each traffic light:

$$\min_{\{t_i \in \mathfrak{T}_i\}_{i=1}^{N+1}} J = k_{\text{t}} J_{\text{t}} + \sum_{i=1}^{N+1} (E_{\text{sta},i} + E_{\text{dyn},i}) \tag{8}$$

where k_{t} is a weighting factor.

[1] An underlying logic goes from the lowest to the highest maximum speed limits within the i-th segment and sets $v_{i,j}$ to the limits from the lower to the highest in order. The sub-segments where $v_{i,j}$ is constrained comprises a set $\mathfrak{J}_{\text{con}} = \{j | v_{i,j} = v_{\max,i,j}\}$. For the sub-segments where $v_{i,j}$ is not constrained, $j \in \mathfrak{J}_{\text{con}}^{\text{c}}$, the logic sets $v_{i,j}$ to an average value, $v_{i,j} = \frac{l_i - \sum_{k\in\mathfrak{J}_{\text{con}}} l_{i,k}}{t_i - t_{i-1} - \sum_{k\in\mathfrak{J}_{\text{con}}} \frac{l_{i,k}}{v_{\max,i,k}}}$.

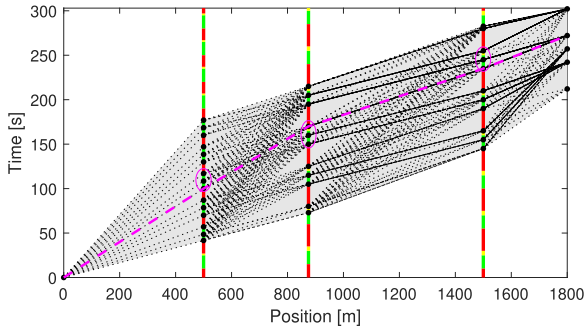

Fig. 2. Minimal-cost path and the corresponding green windows for three signalized intersections: $(s_1, s_2, s_3, s_4) = (500, 850, 1500, 1800)$ m, and $v_{\text{des}} = 8$ m/s.

C. Numerical Algorithm

Feasible set $\mathfrak{T}_i$ represents the green windows at each traffic light that the vehicle can physically reach while obeying maximum and minimum speed limits, as stated in Equation (3). The gray area in Figure 2 implies all the feasible sets in which $\mathfrak{T}_{N+1}$ at the destination is an admissible range in the vicinity of s_{N+1}/v_{des}. To further simplify the problem, we reduce $\mathfrak{T}_i$ to a finite number of points (black dots in Figure 2). In this letter, each green window is discretized into three points,[2] and Dijkstra's algorithm is then applied to search for the path (series of t_i) with the minimal cost J defined in Equation (8); node of graph represents the intersection entering time t_i, and edge paths represent piecewise-constant speed trajectories between s_i. Figure 2 shows one minimal-cost path (magenta dashed line) among all the searched paths (dotted black lines), and the corresponding green windows (magenta circles).

IV. Reference Trajectory Generator

A. Optimization Problem

Equation (2) imposes the interior-point constraints, $s(t_i) = s_i$, $i = 1, \ldots, N$. For analytical treatment, we simplify Equation (1) into a double integrator model by neglecting all resistive forces. By defining a control variable u as F_{req}/m (i.e., required acceleration) and a cost function L as $\frac{1}{2}u^2$ (i.e., control effort), the optimization problem with boundary conditions is formulated as follows:

$$\begin{aligned} \min_{u} \ & J = \int_{t_0}^{t_0+t_{\text{f}}} L(=\frac{1}{2}u^2)\text{dt} \\ \text{s.t.} \ & \dot{x} = f(x,u,t) = [v,u]^T \\ & N_i(x) = s(t_i) - s_i = 0, \ \ i = 1 \cdots N \\ & x_0 = [s_0, v_0]^T, \quad x_{\text{f}} = [s_{\text{f}}, v_{\text{f}}]^T \end{aligned} \tag{9}$$

where the subscripts 0 and f indicate initial and final, respectively.

B. Boundary Value Problem (BVP)

From the optimization problem, we use the necessary condition for optimality in [15] to derive a BVP in ordinary differential equations (ODE) (See Appendix A):

[2]We improved the former version of `PreProcTrfLght` in [13] so that it has higher freedom in optimization by introducing multiple points to represent each single green window.

$$\begin{aligned} \text{Given} \quad & s_0 \text{ and } v_0, \\ & \frac{d}{dt}[s, v, \lambda_1, \lambda_2]^T = [v, -\lambda_2, 0, -\lambda_1]^T \\ \text{s.t.} \quad & \lambda_1(t_i^-) = \lambda_1(t_i^+) + \pi_i \text{ and } \lambda_2(t_i^-) = \lambda_2(t_i^+) \\ & s(t_i) = s_i \\ & s(t_{\text{f}}) = s_{\text{f}} \text{ and } \begin{cases} v(t_{\text{f}}) = v_{\text{f}} & \text{if } v(t_{\text{f}}) \text{ is fixed} \\ \lambda_2(t_{\text{f}}) = \lambda_{2,\text{f}} = 0 & \text{if } v(t_{\text{f}}) \text{ is free} \end{cases} \end{aligned} \tag{10}$$

for $i = 1, \ldots, N$. This BVP can be solved to find $(N+2)$ unknown variables (such as $\lambda_1(t_0)$, $\lambda_2(t_0)$, and π_i) that satisfy $(N+2)$ boundary conditions (such as s_{f}, v_{f} or $\lambda_{2,\text{f}}$, and s_i).

C. Analytical Optimal Entering-Speed Solution

By using explicit ODE solutions, we convert the BVP problem above into a system of N linear equations based on continuity conditions of λ_2 (See Appendix B). Optimal entering-speeds at each traffic light $V = [v_1^*, \ldots, v_N^*]^T$ for the given ts can be directly computed by solving the following system, i.e., $\boldsymbol{V}^* = \boldsymbol{A}^{-1}\boldsymbol{Y}$:

$$\underbrace{\begin{bmatrix} y_1 - 2v_0\xi_1^{-1} \\ y_2 \\ \vdots \\ y_{N-1} \\ y_N - k_0 \end{bmatrix}}_{\boldsymbol{Y}\in\mathbb{R}^N} = \underbrace{\begin{bmatrix} a_1 & b_1 & 0 & \cdots & 0 \\ b_1 & a_2 & b_2 & \cdots & 0 \\ 0 & b_2 & a_3 & \ddots & 0 \\ 0 & 0 & \ddots & \ddots & b_{N-1} \\ 0 & 0 & 0 & b_{N-1} & a_N - k_1 \end{bmatrix}}_{\boldsymbol{A}\in\mathbb{R}^{N\times N}} \underbrace{\begin{bmatrix} v_1^* \\ v_2^* \\ \vdots \\ v_{N-1}^* \\ v_N^* \end{bmatrix}}_{\boldsymbol{V^*}\in\mathbb{R}^N} \tag{11}$$

with $a_i = 4(\xi_i^{-1} + \xi_{i+1}^{-1})$, $b_i = 2\xi_{i+1}^{-1}$, $y_i = 6l_i\xi_i^{-2} + 6l_{i+1}\xi_{i+1}^{-2}$, and

$$\begin{cases} (k_0, k_1) = (2v_{\text{f}}\xi_1^{-1}, 0) & \text{if } v(t_{\text{f}}) \text{ is fixed} \\ (k_0, k_1) = (3l_{N+1}\xi_{N+1}^{-2}, \xi_{N+1}^{-1}) & \text{if } v(t_{\text{f}}) \text{ is free} \end{cases} \tag{12}$$

where A matrix is a symmetric tridiagonal matrix.

D. Numerical Optimal Entering-Time Search

The green window generator provides the minimum and maximum limits of the green window at each traffic light, denoted by $t_{\min,i}$ and $t_{\max,i}$. It is necessary to search optimal entering-times $[t_1^*, \ldots, t_N^*]^T$ in each green window to satisfy the desired criteria, including energy and traffic flow perspectives. Similarly as in Appendix B, the cost defined in Equation (9) of the i-th-interval can be expressed as a function of BC_i:

$$J_i^{\text{e}} = 6l_i^2\xi_i^{-3} - 6l_i(v_{i-1}^* + v_i^*)\xi_i^{-2} + 2(v_{i-1}^{*2} + v_{i-1}^* v_i^* + v_i^{*2})\xi_i^{-1} \tag{13}$$

If a CAV drives slowly on a specific road segment as a result of eco-driving, the vehicles behind it may overtake the CAV from an adjacent or the same lane and deteriorate traffic flow. To this end, we also consider the desired speed of the ith road segment, $v_{\text{des},i}$, as follows:

$$J_i^{\text{t}} = (v_{\text{des},i} - l_i\xi_i^{-1})^2/2 \tag{14}$$

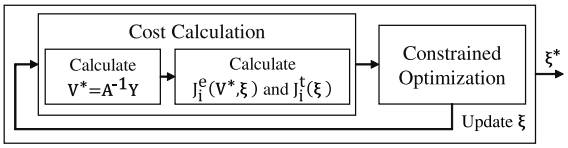

Fig. 3. A schematic diagram of the numerical optimal entering-time search combining with analytical optimal entering-speed solution.

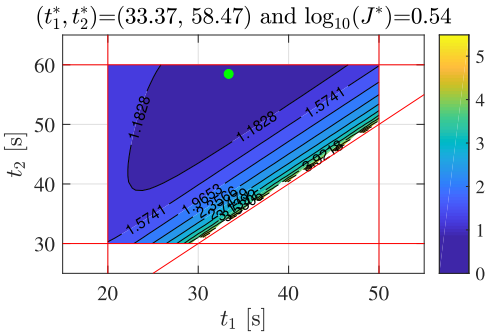

Fig. 4. Contour map of the logarithm of cost J to base 10 with the weighting factor $\alpha = 10^{-0.75}$ in case of two signalized intersections. The green circle, (t_1^*, t_2^*), indicates a point of two optimal entering-times that results in a minimum cost. Red lines indicate inequality constraints.

In summary, we formulate a parametric optimization problem:

$$\begin{aligned} \min_{\boldsymbol{\xi}} \ & J = \sum_{i=1}^{N+1} [(1-\alpha)J_i^{\mathrm{e}} + \alpha J_i^{\mathrm{t}}] \\ \text{s.t.} \ & \boldsymbol{Y} = \boldsymbol{A}\boldsymbol{V}^* \\ & \boldsymbol{T}_{\mathbf{min}} \le \boldsymbol{A}_{\mathbf{ineq}}\boldsymbol{\xi} \le \boldsymbol{T}_{\mathbf{max}} \\ & -\boldsymbol{\xi} \le 0 \end{aligned} \tag{15}$$

where $\boldsymbol{\xi} = [\xi_1, \ldots, \xi_N]^T$, $\boldsymbol{T}_{\mathbf{min}} = [t_{\min.1}, \ldots, t_{\min.N}]^T$, $\boldsymbol{T}_{\mathbf{max}} = [t_{\max.1}, \ldots, t_{\max.N}]^T$, $\boldsymbol{A}_{\mathbf{ineq}}$ is a lower unitriangular matrix (elements are all 1), and α is a weighting factor.

E. Discussion

Using the optimal entering-speed solution, we can calculate the cost and eventually find optimal entering-times while satisfying a series of green windows, as shown in Figure 3.

To illustrate, we consider the simple example where there are two signalized intersections located at 300 and 600 m, respectively. The CAV intends to pass through these two intersections in green windows [20, 50] and [30, 60] s, respectively, and to arrive at 1000 m in 100 s. Figure 4 shows the cost contour map with one specified weighting factor ($\alpha = 10^{-0.75}$), where $v_{\mathrm{des}.1} = v_{\mathrm{des}.2} = v_{\mathrm{des}.3} = 10$ m/s. Depending on the α value, the cost contour map differs as the one perspective is more favored than the other, e.g., the value of $\alpha = 0$ favors the energy perspective only. The value of $\alpha = 10^{-0.75}$ can find a point of two optimal entering-times (green circle) that balances the two perspectives, as shown in Figure 4.

Increasing the weighting factor from $\alpha = 0$ to $\alpha = 1$, we can see the trade-off between minimizing energy and traffic flow costs in Figure 5. Increasing α increases energy cost but decreases traffic flow cost. For example, when $\alpha = 10^{-0.75}$ (the cost contour is shown in Figure 4), the traffic cost is reduced from 1 to 0.2, but the energy cost is increased from 0.55 to 0.7. Figure 5 also shows how optimal entering-times

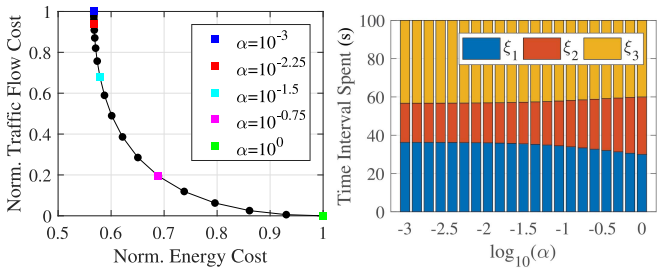

Fig. 5. Trade off between the two normalized costs (left) and optimal entering-times (right), as the weighting factor α increases. Note that $t_1 = \xi_1$, $t_2 = \xi_1 + \xi_2$, and $t_f = \xi_1 + \xi_2 + \xi_3$.

vary with the increase in α. Although the lengths of road segments 1 and 2 are the same, the CAV allocates more time on road segment 1 than on road segment 2 in order to minimize energy cost. This eco-driving behavior on road segment 1 may be uncomfortable for vehicles behind and result in a negative impact on traffic flow upstream (e.g., the CAV brakes due to the cut-in of surrounding vehicles and causes a traffic jam). Note that total travel time is the same because time spent on road segment 2 is shortened.

V. Simulation Study

A. High-Fidelity Simulation Framework

Argonne has developed a new simulation framework called RoadRunner [16] to realistically and accurately evaluate the energy impacts of CAV eco-driving by deploying high-fidelity powertrain models and real-world road attributes provided by the HERE company. We assumed a free-flow situation to study a pure impact of a long communication range on a CAV. A battery electric vehicle is considered, and each CAV is compared with the baseline case of a human-driven vehicle (HV) using the following quantitative measures such as energy savings (ES) and travel time savings (TTS):

$$\mathrm{ES} = (E_{\mathrm{HV}} - E_{\mathrm{CAV}})/E_{\mathrm{HV}}, \mathrm{TTS} = (T_{\mathrm{HV}} - T_{\mathrm{CAV}})/T_{\mathrm{HV}} \tag{16}$$

where E is energy consumption, and T is travel time.

A testing scenario setup procedure is as follows: (1) define a planned route in HERE's digital map, (2) extract and use road attributes (e.g., maximum speed limits, intersection type and location) to build RoadRunner environments, and (3) set the SPaT of each traffic light. We selected four real-world urban routes in the Chicago area. Moreover, we generated six cases for each route by adding the offset to baseline SPaT setup as the timing when the vehicle starts from the origin changes the green/yellow/red sequencing of traffic lights.

B. Speed Planners for CAVs

In our previous work, we presented a real-time speed planner with DSRC-V2I assuming the communication range of 250 meters, and we showed its effectiveness in RoadRunner [8]. In the proposed speed planner with C-V2I, the communication range is set to 1 km so that the speed planner can connect multiple traffic lights within that range. The green window selector is triggered to update the series of green windows when a new intersection comes within the C-V2I communication range when the vehicle is passing through an intersection. Note that if the last connected intersection is a traffic light, v_{f} is

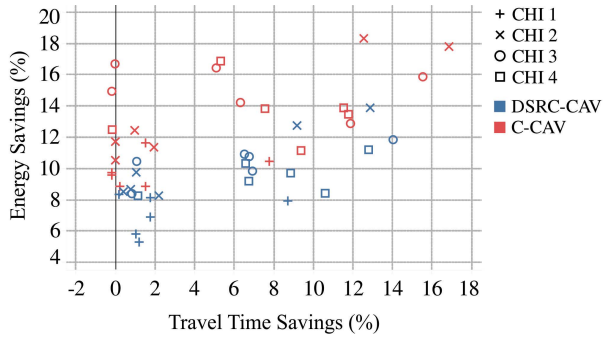

Fig. 6. Energy and travel time savings of all CAVs for four real-world urban routes with six SPaT cases. Each shape indicates a particular route, so there are six points with the same shape due to the six SPaT cases.

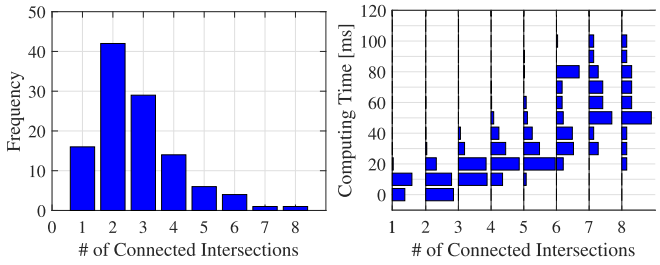

Fig. 7. Frequency distribution of the number of connected intersections (horizontal histogram on the left) and frequency distribution of computing time for one execution of the speed planner with C-V2I, depending on the number of connected intersections (vertical histogram on the right).

free; otherwise, v_f is fixed as zero, and the green window selector is not triggered until the vehicle arrives at the stop light. To estimate accurate energy consumption and travel time, we pre-compute the speed reference trajectory as described above and provide it to the RoadRunner CAVs in a feed-forward way. In summary, two types of planners for CAVs are considered:

- DSRC-CAV: speed planner with DSRC-V2I
- C-CAV[3]: speed planner with C-V2I.

C. Results and Discussion

Figure 6 shows that all CAVs can achieve more than 5% energy savings without increasing travel time over HVs. In Figure 6, as a tuple (TTS, ES), i.e., data point, is located toward the top right, energy is more saved while travel time is more reduced. Data points are spread broadly because adapting the environment differs depending on the route and SPaT setup. Even for the same route, different SPaT setup changes SPaT information to be received when the vehicle approaches the intersection (i.e., the frequency of approaching red lights differs), which makes a difference in travel time and energy savings. Generally, data points of C-CAVs are located in higher regions of the graph than those of DSRC-CAVs. For the same scenario, C-CAV always outperforms DSRC-CAV. C-CAVs achieve additional 2.7%, 3.4%, 4.8%, and 4.1% in ES improvement on average over six SPaT cases in CHI 1, 2, 3, and 4 routes, respectively, compared to DSRC-CAVs.

C-CAVs take advantage of the increased communication range: They can typically connect two or three intersections and can connect up to eight (see Figure 7). As the number

[3]We tune α in Equation (15) to balance energy and traffic perspectives.

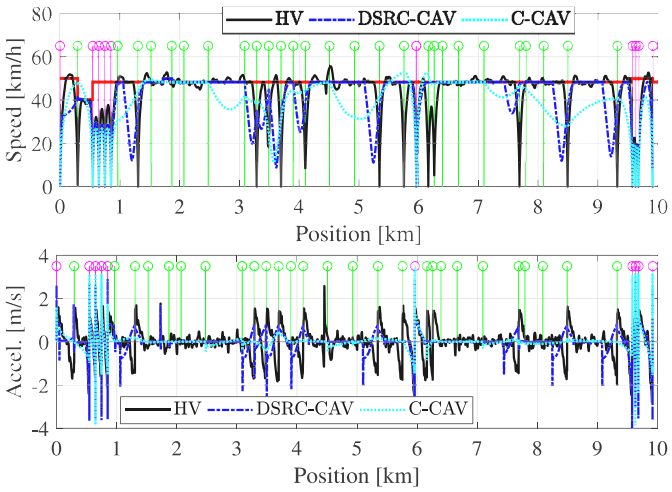

Fig. 8. Speed (top) and acceleration (bottom) trajectories for CHI 3 route with SPAT 3 case. ES of DSRC-CAV and C-CAV are 10.9% and 16.4%, respectively. Vertical magenta lines and vertical green lines indicate stop signs and traffic lights, respectively, and red line indicates maximum speed limit.

of connected intersections increases for the same communication range, the number of paths to be searched in the green window selector and the number of optimal entering-times to be searched in the reference trajectory generator increase. Average computing time for one execution of the speed planner with C-V2I increases with the number of connected intersections, but is guaranteed to be less than 100 ms (see Figure 7). If the C-V2I range decreases up to DSRC-V2I range to satisfy computation requirement, additional ES is expected to monotonically decrease.

As shown in Figure 8, speed and acceleration trajectories differ depending on whether the vehicle is an HV, DSRC-CAV, or C-CAV. At red traffic lights, an HV decelerates and stops, then accelerates until it reaches the cruise speed when the traffic light turns green. On the other hand, DSRC-CAVs activate the eco-approach mode 250 meters before the location of red traffic lights so that they can energy-efficiently pass through intersections on the next green traffic light. Because of the increased communication range, C-CAVs can prepare for passing through multiple intersections using the richer SPaT information received, which results in smoother trajectories that change speed and acceleration as little as possible. It is especially noteworthy that C-CAVs can avoid the driving series consisting of eco-cruise, eco-approach, eco-acceleration, and eco-cruise frequently done by DSRC-CAVs when between 7 and 9.5 km of an approaching red traffic light. Instead, they drive at a lower speed in order to ultimately catch the green light windows of upcoming multiple traffic lights. These driving behaviors can take advantage of reducing aerodynamic drag losses.

VI. Conclusion and Future Work

In this letter, we proposed a hierarchical speed planner with C-V2I that can connect to multiple intersections and verified its feasibility and effectiveness. The hierarchical structure, based on an analytical approach, improves computational efficiency in order to compute and update reference trajectories rapidly, which enables it to properly respond to

dynamically changing situations. The increased number of connected intersections allows CAVs to change speed as seldom as possible, resulting in smoother acceleration and enabling it to pass through all intersections on a green light. This in turn leads to further energy savings compared to the speed planner using limited information. The proposed speed planner is universal, so it can be easily applied to any type of vehicle - internal combustion engine vehicles, hybrids, etc.

In the future, we would like to implement the proposed speed planner in real time in a closed-loop way integrating with collision-free trajectory planning, and validate it for expanded scenarios, including car-following situations. Furthermore, we could perform a sensitivity analysis of C-V2I range to systematically investigate a trade-off between energy optimality and computational efficiency, and consider the existing control approaches that utilize different communication methods for a comparison.

APPENDIX A
BVP DERIVATION

The Hamiltonian H is defined as: $H = L + \lambda^T f = u^2/2 + \lambda_1 v + \lambda_2 u$, where λ_1 and λ_2 are the position and speed co-states, respectively. An optimal control policy is: $H_u = 0 \rightarrow u = -\lambda_2$. The co-state dynamics with jump conditions are: $\dot{\lambda} = -H_x^T = [0, -\lambda_1]^T$ with $\lambda(t_i^-) = \lambda(t_i^+) + \pi_i N_x = \lambda(t_i^+) + [\pi_i, 0]^T$, which implies that λ_1 must have a discontinuity with jump parameter π_i at t_i, whereas λ_2 is always continuous (u is also always continuous). Note that the final condition for free v_f is: $\lambda_2(t_\mathrm{f}) = \frac{\partial h}{\partial v}(t_\mathrm{f}) = 0$, where h is a terminal constraint.

APPENDIX B
CONTINUITY CONDITIONS

Let us define the travel time of the i-th road segment as $\xi_i = t_i - t_{i-1}$, where $\sum_{i=1}^{N+1} \xi_i = t_{N+1} = t_\mathrm{f}$ with $t_0 = 0$, and $\sum_{i=1}^{N+1} l_i = s_{N+1} = s_\mathrm{f}$ with $s_0 = 0$. If the boundary condition (BC) of the i-th road segment is set to $\mathrm{BC}_i = (v_{i-1}, v_i, l_i, \xi_i)$, unknown variables $\lambda_{1.i-1}$ and $\lambda_{2.i-1}$ can be explicitly derived as functions of BC_i: $\lambda_{1.i-1} = -12 l_i \xi_i^{-3} + 6(v_{i-1} + v_i)\xi_i^{-2}$ and $\lambda_{2.i-1} = -6 l_i \xi_i^{-2} + 2(2v_{i-1} + v_i)\xi_i^{-1} = f_1(\mathrm{BC}_i)$. As λ_2 is a linear function of time, $\lambda_2(t_i)$ is the following: $\lambda_{2.i} = 6 l_i \xi_i^{-2} - 2(v_{i-1} + 2v_i)\xi_i^{-1} = f_2(\mathrm{BC}_i)$. Note that $\lambda_{1.i} = \lambda_{1.i-1}$.

To achieve optimality, λ_2 must be continuous: $\lambda_2(t_i^+) - \lambda_2(t_i^-) = f_1(\mathrm{BC}_{i+1}) - f_2(\mathrm{BC}_i) = 0$, where $s_{N+1} = s_\mathrm{f}$, and $v_{N+1} = v_\mathrm{f}$ if $v(t_\mathrm{f})$ is fixed, but $v_{N+1} = (3l_{N+1}\xi_{N+1}^{-1} - v_N)/2$ if $v(t_\mathrm{f})$ is free. The condition of free $v(t_\mathrm{f})$ is derived by $f_2(\mathrm{BC}_{N+1}) = 0$.

ACKNOWLEDGMENT

The authors would like to thank David Anderson of the DOE Office of Energy Efficiency and Renewable Energy (EERE) for his important role in establishing the project concept, advancing implementation, and providing ongoing guidance.

DISCLAIMER

REFERENCES

[1] J. Guanetti, Y. Kim, and F. Borrelli, "Control of connected and automated vehicles: State of the art and future challenges," *Annu. Rev. Control*, vol. 45, pp. 18–40, Jan. 2018.

[2] A. Vahidi and A. Sciarretta, "Energy saving potentials of connected and automated vehicles," *Transp. Res. C, Emerg. Technol.*, vol. 95, pp. 822–843, Oct. 2018.

[3] A. Sciaretta, G. De Nunzio, and L. L. Ojeda, "Optimal ecodriving control: Energy-efficient driving of road vehicles as an optimal control problem," *IEEE Control Syst.*, vol. 35, no. 5, pp. 71–90, Oct. 2015.

[4] Q. Lin *et al.*, "Minimize the fuel consumption of connected vehicles between two red-signalized intersections in urban traffic," *IEEE Trans. Veh. Technol.*, vol. 67, no. 10, pp. 9060–9072, Oct. 2018.

[5] M. A. S. Kamal, M. Mukai, J. Murata, and T. Kawabe, "Model predictive control of vehicles on urban roads for improved fuel economy," *IEEE Trans. Control Syst. Technol.*, vol. 21, no. 3, pp. 831–841, May 2013.

[6] S. E. Li, S. Xu, X. Huang, B. Cheng, and H. Peng, "Eco-departure of connected vehicles with V2X communication at signalized intersections," *IEEE Trans. Veh. Technol.*, vol. 64, no. 12, pp. 5439–5449, Dec. 2015.

[7] N. Wan, A. Vahidi, and A. Luckow, "Optimal speed advisory for connected vehicles in arterial roads and the impact on mixed traffic," *Transp. Res. C, Emerg. Technol.*, vol. 69, pp. 548–563, Aug. 2016.

[8] J. Han, D. Karbowski, and N. Kim, "Closed-form solutions for a real-time energy-optimal and collision-free speed planner with limited information," in *Proc. Amer. Control Conf. (ACC)*, Denver, CO, USA, Jul. 2020, pp. 268–275.

[9] G. Mahler and A. Vahidi, "An optimal velocity-planning scheme for vehicle energy efficiency through probabilistic prediction of traffic-signal timing," *IEEE Trans. Intell. Transp. Syst.*, vol. 15, no. 6, pp. 2516–2523, Dec. 2014.

[10] G. De Nunzio, C. Canudas de Wit, P. Moulin, and D. Di Domenico, "Eco-driving in urban traffic networks using traffic signal information," in *Proc. 52nd IEEE Conf. Decis. Control*, Florence, Italy, Dec. 2013, pp. 892–898.

[11] S. Bae, Y. Choi, Y. Kim, J. Guanetti, F. Borrelli, and S. Moura, "Real-time ecological velocity planning for plug-in hybrid vehicles with partial communication to traffic lights," in *Proc. IEEE 58th Conf. Decis. Control (CDC)*, Nice, France, Dec. 2019, pp. 1279–1285.

[12] C. Sun, J. Guanetti, F. Borrelli, and S. J. Moura, "Optimal eco-driving control of connected and autonomous vehicles through signalized intersections," *IEEE Internet Things J.*, vol. 7, no. 5, pp. 3759–3773, May 2020.

[13] D. Shen, D. Karbowski, and A. Rousseau, "A minimum principle-based algorithm for energy-efficient eco-driving of electric vehicles in various traffic and road conditions," *IEEE Trans. Intell. Veh.*, vol. 5, no. 4, pp. 725–737, Dec. 2020.

[14] X. He, H. X. Liu, and X. Liu, "Optimal vehicle speed trajectory on a signalized arterial with consideration of queue," *Transp. Res. C, Emerg. Technol.*, vol. 61, pp. 106–120, Dec. 2015.

[15] A. E. Bryson and Y.-C. Ho, *Applied Optimal Control: Optimization, Estimation, and Control*. Washington, DC, USA: CRC Press, 1975.

[16] N. Kim, D. Karbowski, and A. Rousseau, "A modeling framework for connectivity and automation co-simulation," SAE Technical Paper 2018-01-0607, Apr. 2018. [Online]. Available: https://doi.org/10.4271/2018-01-0607